Cell-free reconstitution reveals the molecular mechanisms for the initiation of secondary siRNA biogenesis in plants

Yuriki Sakurai[a,b,1], Kyungmin Baeg[a,1], Andy Y. W. Lam[a,b], Keisuke Shoji[a], Yukihide Tomari[a,b,2], and Hiro-oki Iwakawa[a,c,2]

[a]Institute for Quantitative Biosciences, The University of Tokyo, Bunkyo-ku, Tokyo 113-0032, Japan; [b]Department of Computational Biology and Medical Sciences, Graduate School of Frontier Sciences, The University of Tokyo, Bunkyo-ku, Tokyo 113-0032, Japan; and [c]Precursory Research for Embryonic Science and Technology (PRESTO), Japan Science and Technology Agency (JST), Saitama 332-0012, Japan

Edited by R. Scott Poethig, University of Pennsylvania, Philadelphia, PA, and approved June 23, 2021 (received for review February 11, 2021)

Secondary small interfering RNA (siRNA) production, triggered by primary small RNA targeting, is critical for proper development and antiviral defense in many organisms. RNA-dependent RNA polymerase (RDR) is a key factor in this pathway. However, how RDR specifically converts the targets of primary small RNAs into double-stranded RNA (dsRNA) intermediates remains unclear. Here, we develop an in vitro system that allows for dissection of the molecular mechanisms underlying the production of trans-acting siRNAs, a class of plant secondary siRNAs that play roles in organ development and stress responses. We find that a combination of the dsRNA-binding protein, SUPPRESSOR OF GENE SILENCING3; the putative nuclear RNA export factor, SILENCING DEFECTIVE5, primary small RNA, and Argonaute is required for physical recruitment of RDR6 to target RNAs. dsRNA synthesis by RDR6 is greatly enhanced by the removal of the poly(A) tail, which can be achieved by the cleavage at a second small RNA-binding site bearing appropriate mismatches. Importantly, when the complementarity of the base pairing at the second target site is too strong, the small RNA–Argonaute complex remains at the cleavage site, thereby blocking the initiation of dsRNA synthesis by RDR6. Our data highlight the light and dark sides of double small RNA targeting in the secondary siRNA biogenesis.

RNA silencing | microRNA | secondary siRNA | trans-acting siRNA | phased siRNA

MicroRNAs (miRNAs) and small interfering RNAs (siRNAs) are critical for the regulation of a broad range of biological functions across the kingdoms of life. Such small RNAs are processed from hairpin RNAs or double-stranded RNAs (dsRNAs) by the RNase III Dicer or Dicer-like proteins (DCLs) (1, 2). Small RNAs cannot function alone and form effector ribonucleoprotein complexes called RNA-induced silencing complexes (RISCs) with Argonaute (AGO) proteins to exert their functions (1, 3). RISCs bind to target RNAs via base complementarity. When the central region of the base pairing between small RNA and the target site is complementary, RISCs cleave the target RNA through the intrinsic slicing activity of AGO. Even in the presence of central mismatches, RISCs can recruit additional regulatory factors, thereby inducing messenger RNA (mRNA) decay and/or translational repression (2, 4–6).

In addition, many organisms, including plants, fungi, and worms, harness a powerful mechanism that amplifies the initial RNA silencing signal, in which target RNAs of primary small RNAs trigger the production of secondary siRNAs (7). RNA-dependent RNA polymerase (RDR), which converts target RNAs into dsRNAs, is central to secondary siRNA production (1, 8–11). RDR-mediated dsRNA production and subsequent Dicer-mediated processing trigger the spreading of silencing from the initial cleavage site targeted by primary small RNA-loaded RISC toward flanking sequences that lie 5′ or 3′ in the target transcript. Production of secondary siRNAs is required for regulation of endogenous gene expression as well as defense against viruses and transposons (1, 2, 12). However, the molecular details of these critical silencing amplification steps are not well understood due to their complexity.

Phased siRNAs (phasiRNAs) are plant secondary siRNAs that regulate development and stress responses. PhasiRNA biogenesis is triggered by the recruitment of primary miRNA-loaded RISCs, the majority of which are 22-nt miRNA-loaded AGO1-RISCs, to the phasiRNA generating (PHAS) precursor transcripts (PHAS transcripts) (13–15). Trans-acting siRNAs (tasiRNAs) are a subtype of phasiRNAs. As the name suggests, tasiRNAs predominantly suppress mRNAs other than the original tasiRNA generating (TAS) precursor transcripts (TAS transcripts) in trans. After RISC-mediated cleavage or binding, RDR6 synthesizes the complementary strand of the precursor transcripts (16, 17). The resulting long dsRNA is then processed by DCLs into ∼21- or 24-nt secondary siRNAs, with the phase determined by the initial miRNA-guided cleavage site (15, 18, 19). In addition to these factors, two proteins, known as the dsRNA-binding protein, SUPPRESSOR OF GENE SILENCING3 (SGS3) and a putative RNA export protein, SILENCING DEFECTIVE5 (SDE5), are required for tasiRNA biogenesis (20–23). It has been reported that SGS3 forms membrane-associated cytoplasmic foci named siRNA bodies with

Significance

Double-stranded RNA (dsRNA) synthesis by RNA-dependent RNA polymerase (RDR) is a critical step in secondary small interfering RNA (siRNA) biogenesis. However, how RDR specifically converts the targets of primary small RNAs into dsRNA intermediates remains unclear. Here, we developed an in vitro system that recapitulates the production of secondary siRNAs that are physiologically important in plants. Leveraging this system, we showed that a combination of four plant factors promotes physical recruitment of RDR6 to the target RNA. Moreover, we found that dsRNA synthesis by RDR6 is enhanced by the removal of the poly(A) tail, which is achieved by cleavage at another small RNA-binding site bearing appropriate mismatches. Our data elucidate the molecular events necessary for secondary siRNA biogenesis in plants.

Author contributions: Y.S., K.B., and H.-o.I. designed research; Y.S., K.B., and A.Y.W.L. performed research; Y.S., K.B., A.Y.W.L., K.S., Y.T., and H.-o.I. analyzed data; Y.S., K.B., A.Y.W.L., Y.T., and H.-o.I. wrote the paper; and Y.T. and H.-o.I. supervised the project.

The authors declare no competing interest.

This article is a PNAS Direct Submission.

[1]Y.S. and K.B. contributed equally to this work.

[2]To whom correspondence may be addressed. Email: tomari@iqb.u-tokyo.ac.jp or iwakawa@iqb.u-tokyo.ac.jp.

This article contains supporting information online at https://www.pnas.org/lookup/suppl/doi:10.1073/pnas.2102889118/-/DCSupplemental.

Published July 30, 2021.

RDR6 and AGO7, a special AGO protein able to trigger tasiRNA biogenesis by forming RISC with 21-nt miR390 (24–27). SGS3 is also known to physically interact with RISCs in the presence of precursor transcripts, including miR390-loaded AGO7 (28) and 22-nt miR173-loaded AGO1-RISC (29). Although no physical interaction has been detected between SDE5 and RISCs, epistasis analysis places SDE5 functions between SGS3 and RDR6 during tasiRNA biogenesis (30). However, due to the lack of a biochemical framework that allows dissection of the complex phasi/tasiRNA pathway, the molecular mechanism of phasi/tasiRNA biogenesis driven by RISCs, SDE5, and SGS3 remains obscure.

PHAS/TAS loci are divided into two classes—dubbed "one hit" and "two hit"—based on the number of primary miRNA binding sites. Most PHAS/TAS transcripts, including TAS1/2 RNA in *Arabidopsis*, have a single 22-nt miRNA binding site (15). Although a few two-hit precursors have been predicted, only TAS3 is experimentally validated, which is evolutionarily conserved from moss to flowering plants and considered the origin of PHAS/TAS precursors (31). TAS3 carries two 21-nt miR390 target sites (31); the 5′ proximal site has a central mismatch in most species, whereas the central region of the 3′ proximal site is perfectly complementary to miR390 and is thereby cleaved by AGO7-RISC (31–33) (Fig. 1*A*). Although the 3′ miR390-binding site is not essential for secondary siRNA biogenesis (34), it is important for determining the correct phase to generate functional tasiRNAs. For example, the seventh (5′D7 [+]) and eighth (5′D8 [+]) tasiRNAs relative to the 3′ miR390-guided cleavage site regulate AUXIN RESPONSE FACTOR3 and 4 (35, 36) (Fig. 1*A*). The base pairing between the 3′ site and miR390 has evolutionarily conserved mismatches at the 3′ end region of miR390 (Fig. 1*A*) (31). However, the significance of these mismatches remains unclear.

Another unsolved issue is how the 3′ poly(A) tail impacts the initiation of phasi/tasiRNA biogenesis. Recombinant RDR6 has a strong preference for non–poly(A)-tailed 3′ ends as initiation sites (17). This is supported by several in vivo observations that inefficient termination of transcription, which produces "read-through" mRNAs lacking poly(A) tail or with a short poly(A) tail, induces strong posttranscriptional gene silencing (PTGS) (37, 38). In contrast, the complementary strands of one-hit precursors, TAS1/2, with 5′ poly(U) accumulate in the *dcl2/3/4* mutant (39), indicating that RDR6 can start dsRNA conversion from the 3′ end of polyadenylated TAS1/2. These conflicting results leave the role of the poly(A) tail in tasiRNA biogenesis unclear.

Here, we reconstitute the tasiRNA biogenesis pathway in a tobacco cell-free system, allowing for dissection of this pathway. We showed that a combination of 1) initiator RISCs, 2) SGS3, and 3) SDE5 is required for physical recruitment of RDR6 to the template RNA. Furthermore, we find that the removal of the poly(A) tail from the template RNAs greatly enhances the efficiency of complementary RNA synthesis by RDR6 in both the TAS3 and TAS1 tasiRNA biogenesis pathways. Moreover, we find that the evolutionarily conserved mismatches between miR390 and the 3′ binding site are essential for the initiation of dsRNA synthesis by promoting rapid release of AGO7-RISC from the cleavage site. Our study provides mechanistic understanding of RDR-mediated secondary siRNA biogenesis in plants.

Results

Reconstitution of the TAS3 tasiRNA Biogenesis Pathway In Vitro. We developed an in vitro system to dissect the plant secondary siRNA biogenesis pathway. We selected the TAS3 pathway as a model because this pathway is well conserved and essential for proper plant development (31, 40). We started with a tobacco Bright Yellow 2 (BY-2) cell lysate, specifically the 17,000 × *g* supernatant, which has been successfully used to study plant RISC assembly and function (29, 41–45). In order to check whether endogenous tasiRNA biogenesis factors in the naïve tobacco cell extract are sufficient for secondary siRNA production, we added TAS3 RNA to the extract (*SI Appendix*, Fig. S1*A*). However, 5′D7 (+)—the most abundant TAS3 tasiRNA—was not detected by northern blotting (*SI Appendix*, Fig. S1*A*), suggesting a lack of tasiRNA factors in the naïve tobacco cell extract. Indeed, TAS3 mRNA remained intact without cleavage (*SI Appendix*, Fig. S1*A*), suggesting that this naïve extract contains insufficient levels of functional AGO7-RISC. We therefore in vitro translated mRNAs carrying tasiRNA factors fused to Flag tags (AtAGO7, AtSGS3, AtSDE5, and AtRDR6) in the cell-free system. We added miR390 duplexes, which are bound to AtAGO7 to form RISC, before incubation with TAS3 RNA (Fig. 1 *B* and *C* and *SI Appendix*, Fig. S1*B*). We did not supplement DCLs since previous reports observed endogenous DCL activities in BY-2 lysate (46, 47). Supplementation of tasiRNA factors efficiently triggered tasiRNA production from cleaved TAS3 fragments (Fig. 1*C* and *SI Appendix*, Fig. S1*C*). To check the contribution of each supplemented factor, we systematically omitted miR390 or mRNAs corresponding to each tasiRNA factor, one at a time, from the reaction. Removal of TAS3 mRNA, AtAGO7 mRNA, miR390 duplex, or AtSDE5 mRNA greatly compromised tasiRNA production (Fig. 1 *C* and *D* and *SI Appendix*, Fig. S1 *A* and *D*), so we supplemented naïve BY-2 cell extract with all of these factors as we moved forward with further analysis.

Although we successfully detected two TAS3 tasiRNAs, 5′D7 (+) and 5′D8 (+) (Fig. 1*C* and *SI Appendix*, Fig. S1 *C* and *D*), it was still unclear whether the pattern of in vitro expressed tasiRNAs was similar to in vivo production. To ascertain this, we sequenced the small RNAs produced in our in vitro system and compared them to TAS3a tasiRNAs produced in wild-type *Arabidopsis* seedlings (Col-0) but lost in *sgs3* mutant plants (*sgs3-11*) (Fig. 1*E*). Small RNAs generated in vitro mapped between the two miR390 binding sites, but only in the presence of both miR390 duplex and AGO7 (Fig. 1*E*), suggesting that the mapped small RNAs were bona fide miR390-AGO7-triggered tasiRNAs. Interestingly, although relatively high levels of 24-nt small RNAs mapped to the TAS3a RNA due to robust DCL3-like activity in BY-2 cell extracts (*SI Appendix*, Fig. S1*E*) (46, 47), the position of the most prominent 21-nt tasiRNA hotspot was common between in vivo and in vitro processing (Fig. 1*E*). Taken altogether, the system we developed accurately recapitulates TAS3 tasiRNA biogenesis in vitro. We also tested that this in vitro system also synthesizes dsRNAs and produces tasiRNAs from the one-hit precursor TAS1a that has a binding site for 22-nt miR173-AGO1 RISC (*SI Appendix*, Fig. S2).

SDE5 and SGS3 Function at the dsRNA Conversion Step. We next sought to investigate the exact steps at which SDE5 and SGS3 function in tasiRNA biogenesis. Given that the removal of SGS3 or SDE5 mRNA from the reaction had no effect on AGO7-mediated target cleavage (Fig. 1*C*), we hypothesized that both factors function upstream of dsRNA synthesis. However, the antisense strand of TAS3 RNA was barely detected by northern blotting even in the presence of exogenous AGO7-RISC and SDE5 (Fig. 2*A*), presumably due to rapid processing of dsRNAs into siRNAs by endogenous DCL activities. To stabilize dsRNA intermediates so that we could detect them and resolve the role of SGS3 and SDE5, we added Flock House virus (FHV) B2 protein, which is known to inhibit dsRNA processing by DCLs (48–50) (Fig. 2*B*). Addition of FHV B2 protein strongly inhibited tasiRNA processing, leading to accumulation of dsRNA intermediates (Fig. 2 *A* and *B*), while having no effect on RISC-mediated target cleavage. The size of the antisense strand is in line with a previous report, having the sequence from the third nucleotide of the 3′ cleaved site to the one nucleotide upstream of the 3′ end of the 5′ miR390 binding site (Fig. 2*B*) (51). FHV B2 exposure in the absence of SDE5 supplementation showed decreased accumulation of dsRNA intermediates (Fig. 2*A*), indicating that SDE5 functions at the dsRNA conversion step. Since endogenous SGS3 in BY-2 cell extract sufficiently promoted tasiRNA production (Fig. 1 *C* and *D*), we immunodepleted endogenous

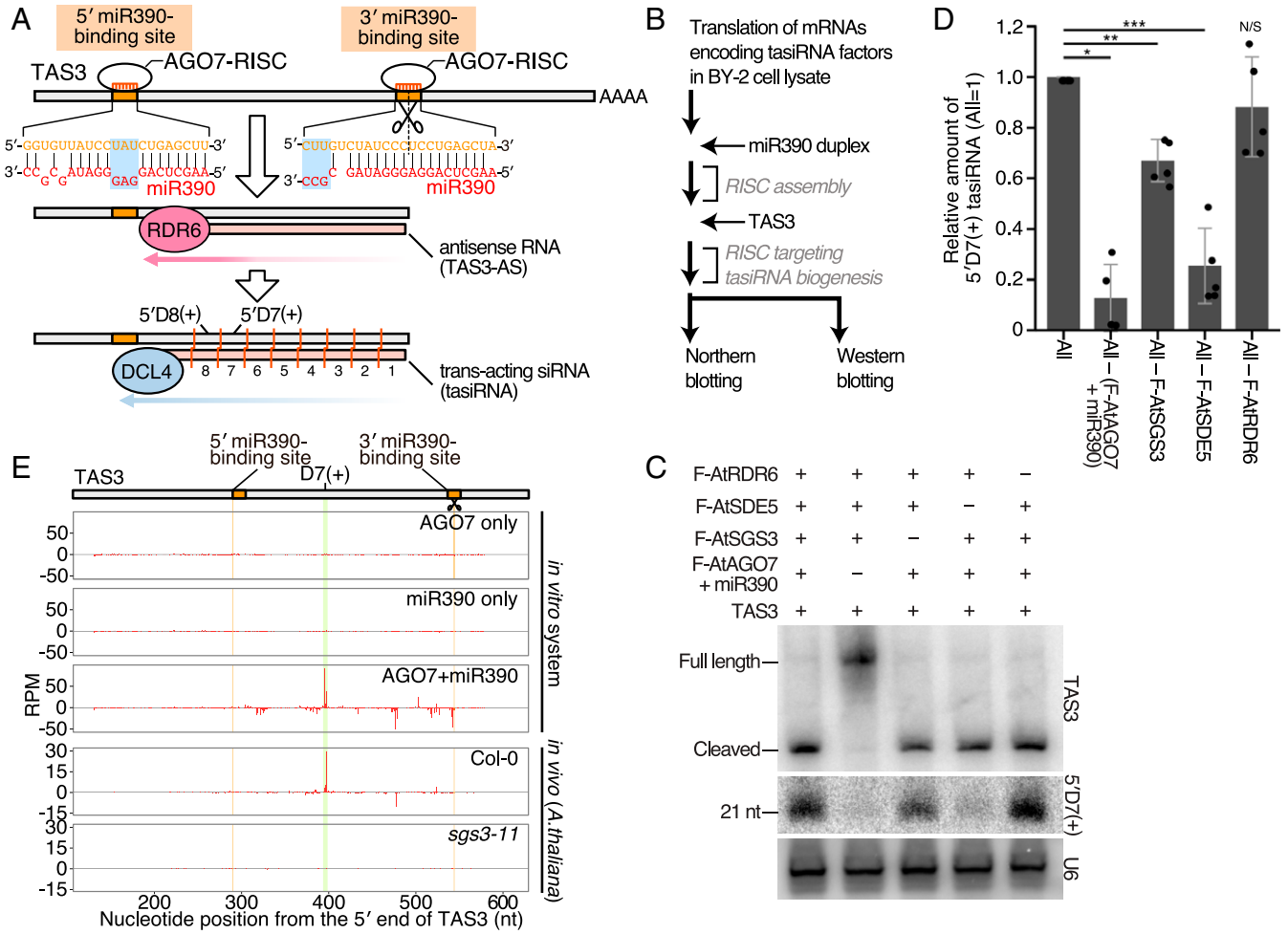

Fig. 1. Recapitulation of the TAS3 tasiRNA biogenesis pathway in vitro. (*A*) Schematic outlining current understanding of the TAS3 tasiRNA biogenesis pathway. AGO7-miR390 complexes target two binding sites in the TAS3 mRNA. The base pairings between miR390 (shown in red) and the 5′ and 3′ binding sites (shown in orange) possess the evolutionarily conserved mismatches (highlighted in light blue) at the central and the 3′ end region, respectively. Following AGO7-RISC–mediated cleavage of the 3′ proximal site, RDR6 converts the 5′ cleaved fragment into dsRNA. The resulting long dsRNA is then processed into 21-nt siRNAs by DCL4. 5′D7 (+) tasiRNA, which is the seventh tasiRNA in register with the cleavage site, is located in the sense strand of the long dsRNA. (*B*) Flowchart of TAS3 tasiRNA biogenesis assay. After in vitro translation of mRNAs encoding tasiRNA factors in BY-2 lysate, miR390 duplex was added to form AGO7-RISC. The TAS3 mRNA was then added to trigger tasiRNA biogenesis. (*C*) In vitro recapitulation of TAS3 tasiRNA biogenesis. tasiRNA biogenesis was performed as outlined in *B*. TAS3 sense RNA and 5′D7 (+) tasiRNA were detected by northern blotting. U6 spliceosomal RNA was used as a loading control. See also *SI Appendix*, Fig. S1*B*. (*D*) Quantification of 5′D7 (+) tasiRNAs in *C*. The band intensity of 5′D7 (+) tasiRNA was normalized to the value of that in the reaction mixture with all tasiRNA factors (*All*). The graphs show the mean ± SD from five technically independent experiments. Bonferroni-corrected *P* values from two-sided paired *t* test are indicated (*$P = 4.92 \times 10^{-4}$, **$P = 3.66 \times 10^{-3}$, ***$P = 1.45 \times 10^{-3}$). (*E*) Distribution of 21-nt siRNAs relative to TAS3a mRNA produced in recapitulated reaction mixtures (AGO7 only, miR390 only, and AGO7 + miR390), in Col-0, and in *sgs3-11* seedlings (top to bottom). The traces indicate the position of the 5′ end for sense siRNAs and antisense siRNAs. The 5′ end of miR390 binding sites and 3′ cleavage sites are indicated by orange lines. In the presence of AGO7-miR390-RISC, siRNAs efficiently mapped between the 5′ and 3′ miR390 binding sites in the TAS3 mRNA. siRNAs mapped to the TAS3 loci in Col-0 but not in the *sgs3-11* mutant. See also *SI Appendix*, Fig. S1*E*.

NtSGS3 using anti-NtSGS3 antibody conjugated beads (*SI Appendix*, Fig. S3*A*). In the resulting SGS3-depleted lysate, tasiRNA and dsRNA accumulation was dramatically decreased (Fig. 2*C* and *SI Appendix*, Fig. S3*A*). To further validate the importance of SGS3 protein in the dsRNA conversion step, we added recombinant AtSGS3 protein (28) into SGS3-depleted or mock-depleted lysates (Fig. 2*C* and *SI Appendix*, Fig. S3*A*). Supplementing recombinant SGS3 protein restored tasiRNA biogenesis as well as complementary strand synthesis in the SGS3-depleted lysate (Fig. 2*C* and *SI Appendix*, Fig. S3*A*), indicating that SGS3 is required for complementary strand synthesis of TAS3. In summary, we conclude that both SDE5 and SGS3 are required for the dsRNA synthesis step.

SGS3 and SDE5 Promote Physical Association between RDR6 and the Target RNA Bound to AGO7-RISC. The requirement for SGS3 and SDE5 at the dsRNA conversion step led us to hypothesize that SGS3 and SDE5, together with AGO7-RISC, form a large complex that recruits RDR6 to the target mRNA. To test this hypothesis, we first investigated physical interactions among SGS3, SDE5, AGO7-RISC, and RDR6. We in vitro translated the mRNAs carrying AtSDE5 with an N-terminal triple influenza hemagglutinin (HA) epitope tag (3×HA-AtSDE5) and 3×FLAG-AtAGO7 in the cell-free system and then performed coimmunoprecipitation experiments using the anti-FLAG antibody (Fig. 2*D*). In the presence of both miR390 and TAS3 RNA, endogenous NtSGS3 and NtRDR6 were specifically coimmunoprecipitated with AtAGO7 (Fig. 2*E*) but not with the negative control, 3×FLAG-β-galactosidase (LacZ) (*SI Appendix*, Fig. S3*B*). Similar results were obtained when NtSGS3 was used as the bait protein (Fig. 2*F*). Thus, AtAGO7, SGS3, and RDR6 are physically associated with each other when miR390 base pairs with TAS3 RNA, in line with previous in vivo data showing that SGS3, AGO7, and RDR6 were colocalized in siRNA bodies (26, 27).

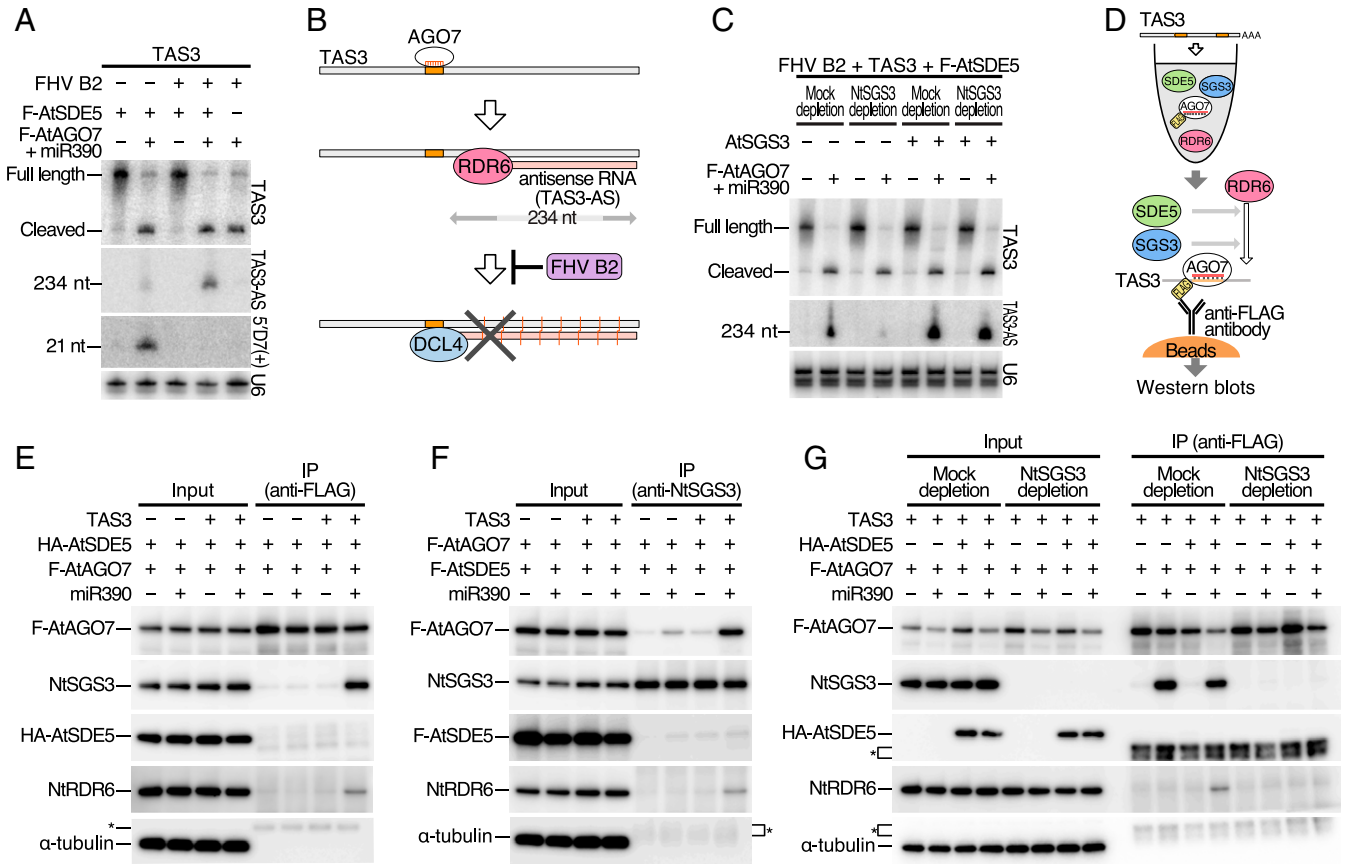

Fig. 2. SGS3 and SDE5 are required for RDR6-mediated dsRNA conversion. (*A*) In vitro synthesis of the complementary strand of TAS3 RNA in the presence or absence of FHV B2. The TAS3 sense RNA, TAS3 antisense RNA (TAS3-AS), and 5′D7 (+) tasiRNA were detected by northern blotting with specific probes. U6 spliceosomal RNA was used as a loading control. In the presence of SDE5, addition of FHV B2 leads to accumulation of the antisense strand of TAS3 mRNA. In contrast, TAS3 antisense strand was barely observed in the absence of SDE5. (*B*) Schematic illustrating FHV B2 function. FHV B2 blocks the dicing reaction, leading to accumulation of dsRNA intermediates generated by RDR6. (*C*) In vitro synthesis of the complementary strand of TAS3 RNA with SGS3-immunodepleted lysate in the presence of FHV B2 protein. TAS3 sense and antisense RNAs were detected by northern blotting with specific probes. U6 spliceosomal RNA was used as a loading control. SGS3 depletion leads to loss of dsRNA accumulation, suggesting that SGS3 is required for RDR6-mediated dsRNA conversion. See also *SI Appendix*, Fig. S3*A*. (*D*) Schematic illustrating coimmunoprecipitation assay using the anti-FLAG antibody. (*E*) Coimmunoprecipitation experiments with 3×FLAG-AtAGO7 (F-AtAGO7). NtRDR6 and NtSGS3 were coimmunoprecipitated with F-AtAGO7, but only in the presence of both TAS3 mRNA and miR390 duplex. F-AtAGO7, 3×HA-AtSDE5 (HA-AtSDE5), NtSGS3, and NtRDR6 were detected by Western blotting. α-tubulin was used as a loading control as well as a negative control for coimmunoprecipitation experiments. The asterisk indicates nonspecific bands. (*F*) Coimmunoprecipitation experiments with NtSGS3. NtRDR6 and F-AtAGO7 were coimmunoprecipitated with NtSGS3 but only in the presence of both TAS3 mRNA and miR390 duplex. F-AtAGO7, 3×FLAG-AtSDE5 (F-AtSDE5), NtSGS3, and NtRDR6 were detected by Western blotting. α-tubulin was used as a loading control as well as a negative control for coimmunoprecipitation experiments. (*G*) Coimmunoprecipitation experiments with F-AtAGO7 in the NtSGS3 or mock-depleted lysate. NtRDR6 was coimmunoprecipitated by F-AtAGO7 but only in the presence of HA-AtSDE5, NtSGS3, miR390 duplex, and TAS3 RNA. α-tubulin was used as a loading control as well as a negative control for coimmunoprecipitation experiments. Asterisks indicate nonspecific bands.

Although the signals were faint, SDE5 also coimmunoprecipitated with SGS3 (Fig. 2*F*). To confirm the interaction between SDE5 and other tasiRNA factors, we used SDE5 as the bait protein. AGO7, SGS3, and RDR6 coimmunoprecipitated with SDE5, the efficiency of which was the highest in the presence of both miR390 and TAS3 RNA (*SI Appendix*, Fig. S3*C*). Thus, although the interactions are weak, SDE5 also physically associated with RDR6 and the TAS3-miR390-AGO7-SGS3 complex. Importantly, when either SGS3 or SDE5 was depleted from the lysate, RDR6 did not coimmunoprecipitate with AGO7 even in the presence of both miR390 and TAS3 RNA, suggesting that both SGS3 and SDE5 are required for promoting the physical association between RDR6 and AGO7-RISC–bound TAS3 RNA (Fig. 2*G*).

The 5′ miR390-Binding Site of TAS3 Facilitates the Interaction between RDR6 and AGO7-RISC. TAS3 RNA carries two evolutionarily conserved miR390 target sites (31) (Fig. 1*A*). As multiple miRNA binding sites often augment silencing activity (5), we investigated the contribution of the two miR390-binding sites on TAS3 to RDR6 recruitment. We prepared three TAS3 RNA variants with mutations in one or both miR390 binding sites (5m3W, 5W3m, and 5m3m) (Fig. 3*A*). These mutations were introduced into target sequence complementary to the seed sequence of miR390 (2 to 8 nt position from the 5′ end), a region that is critical for target binding (Fig. 3*A*). As expected, a TAS3 variant carrying mutations in both miR390 binding sites (5m3m) impaired interaction between NtRDR6 and AGO7-RISC (Fig. 3*B*). Similarly, no interaction was observed between NtRDR6 and AGO7-RISC when the 5′ miR390 binding site mutant (5m3W) was incubated with AGO7-RISC. In contrast, wild-type TAS3 (5W3W) and the 3′ miR390 binding site mutant (5W3m) retained interaction between NtRDR6 and AGO7-RISC (Fig. 3*B*). Thus, the 5′ miR390 binding site is specifically required for the interaction between RDR6 and AGO7-RISC.

Poly(A) Removal by the 3′ Site Cleavage Facilitates TAS3 Complementary Strand Synthesis. Since the 5′ but not the 3′ miR390 binding site, was necessary for RDR6 recruitment to TAS3 mRNA (5W3W and 5W3m), we asked if the 5′ miR390 binding site alone is sufficient for the production of long dsRNAs. Surprisingly, antisense TAS3 was detected only when both miR390 binding sites were wild type (5W3W) (Fig. 3*C*). This result indicates that the 3′ miR390 binding site has a crucial role for RDR6 activity after its recruitment to the AGO7-bound TAS3 mRNA. We wondered why synthesis of the antisense strand of 5W3m is impaired, even though this mutant still recruits RDR6. We previously reported that the poly(A) tail blocks recombinant RDR6-mediated complementary strand RNA synthesis in vitro (17). We therefore hypothesized that removal of the poly(A) tail through cleavage of the 3′ miR390 binding site enhances RDR6 activity. If so, replacement of the poly(A)-tail of 5W3m with a non-poly(A) sequence should support complementary strand synthesis (Fig. 3*A*). Indeed, replacing the poly(A) tail with 140-nt of non-poly(A) sequence promoted complementary strand synthesis (Fig. 3*D*). Since RDR6 recruitment was similar between polyadenylated and non-polyadenylated 5W3m (*SI Appendix*, Fig. S4), the poly(A) tail does not impair RDR6 recruitment but rather blocks the initiation of complementary strand synthesis. Taken together, we conclude that the 3′ miR390 binding site is important for not only determination of the starting position of tasiRNA phasing (34) but also the removal of the poly(A) tail to enhance dsRNA synthesis by RDR6. We also observed a similar enhancement of complementary strand synthesis by poly(A) removal in the TAS1 pathway (*SI Appendix*, Fig. S2 *B* and *D*).

The Mismatches in the 3′ miR390-Binding Site Are Essential to Initiate dsRNA Synthesis by Promoting Rapid Release of AGO7-RISC from the Cleavage Site. *Arabidopsis* TAS3 RNA has mismatches in both 5′ and 3′ miR390-binding sites. The 5′ miR390-binding site has central

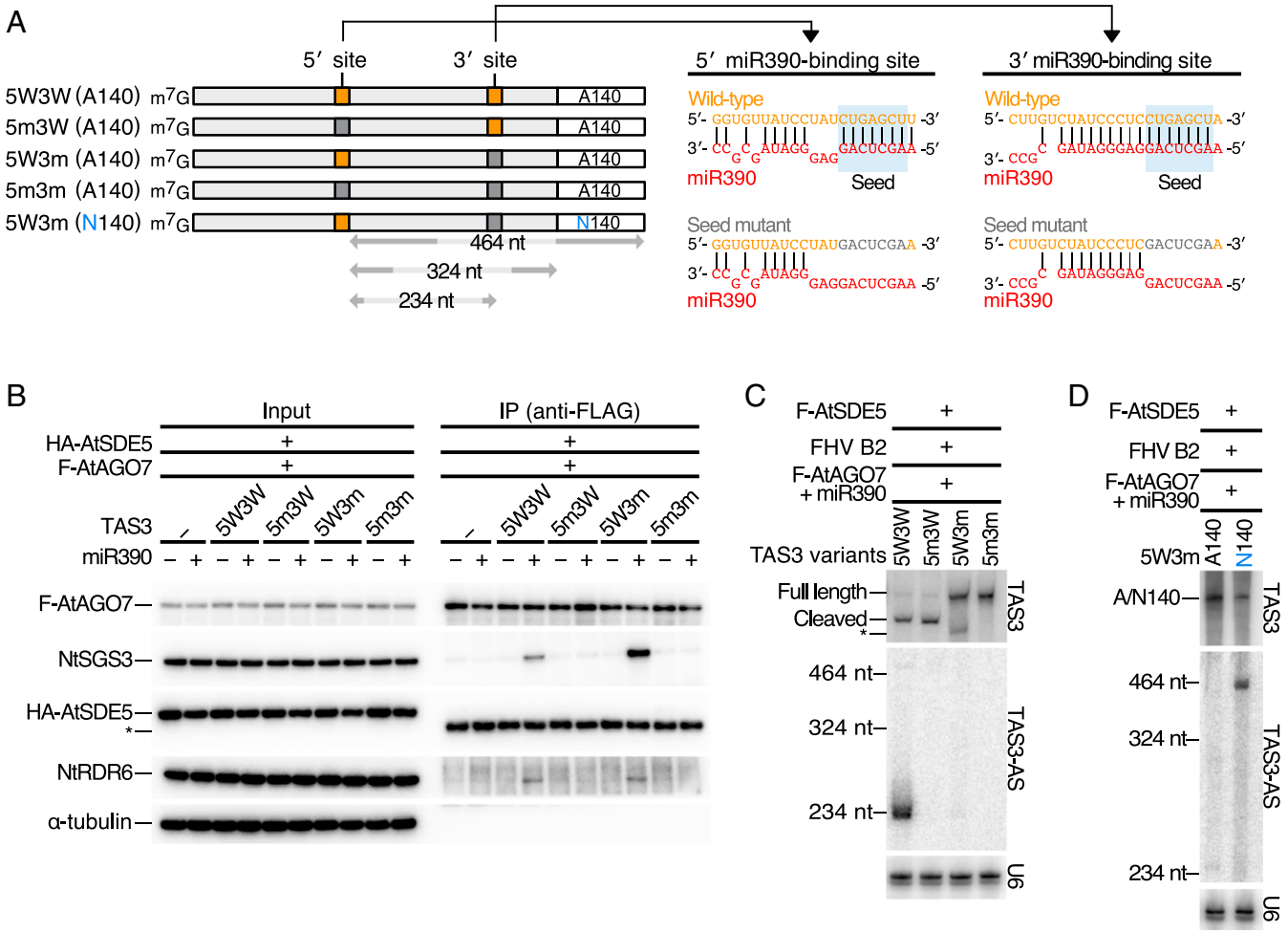

Fig. 3. Roles of each miR390-binding site in TAS3 mRNA. (*A*, *Left*) A schematic illustrating wild-type TAS3 and TAS3 variants with a 140 nt poly(A) tail or 140 nt non-poly(A) sequence at the 3′ end. The orange and gray boxes indicate the wild-type and mutant miR390 binding sites, respectively. (*Right*) The base-pairing configurations between miR390 (shown in red) and the wild-type (highlighted in orange) or mutated (highlighted in gray) miR390 binding sites. The light blue shaded box indicates seed pairing (2 to 8 nt position from the 5′ end of miR390), which is critical for the interaction between RISCs and target RNAs. (*B*) Coimmunoprecipitation experiments with F-AtAGO7 in the presence of TAS3 variants shown in *A*. NtRDR6 and NtSGS3 were coimmunoprecipitated with F-AtAGO7 in the presence of TAS3 mRNAs with the wild-type 5′ miR390 binding site (5W3W-A140 and 5W3m-A140) in a manner dependent on the miR390 duplex. The asterisk indicates nonspecific bands. α-tubulin was used as a loading control as well as a negative control for coimmunoprecipitation experiments. (*C*) In vitro synthesis of the complementary strand of wild-type TAS3 or TAS3 variants in the presence of FHV B2. Both 5′ and 3′ miR390 sites were required for efficient synthesis of the complementary strand. TAS3 sense and antisense RNAs were detected by northern blotting with specific probes. U6 spliceosomal RNA was used as a loading control. The asterisk indicates a degradation intermediate of 5W3m only detected in the presence of AGO7-RISC. (*D*) In vitro synthesis of the complementary strand of the TAS3 variants with mutations in the 3′ miR390 site (5W3m) bearing a 140 nt poly(A) tail or non-poly(A) sequence at the 3′ end. The 140-nt poly(A) tail, but not the non-poly(A) sequence of the same length, inhibited complementary strand synthesis of 5W3m in vitro. TAS3 sense and antisense RNAs were detected by northern blotting with specific probes. U6 spliceosomal RNA was used as a loading control. See also *SI Appendix*, Fig. S3.

mismatches in the base pairing with miR390, while the 3′ miR390-binding site has conserved mismatches in the base pairing with the 3′ end of miR390 (Fig. 4*A*). To examine the importance of these mismatches, we introduced compensatory mutations in the 5′ and 3′ miR390 binding sites that allow full Watson–Crick base pairing with the central and the 3′ end region of miR390, respectively (5P3W and 5W3P; Fig. 4*A*). Although the introduction of compensatory mutations into the 5′ miR390 binding site induced cleavage at the 5′ site in the sense strand, both antisense RNAs with the sequence between the two binding sites and tasiRNAs were efficiently generated from 5P3W (Fig. 4*B*). Thus, the central mismatches in the 5′ miR390 binding site are dispensable for the initiation of dsRNA synthesis. These results are in line with previous transient expression assays with *Nicotiana benthamiana* and the fact that some plant species, including moss *Physcomitrella patens*, have the cleavable 5′ miR390 binding site (33, 34). Note that an additional band was observed above the ∼234-nt antisense strand in the reaction mixture containing 5P3W (Fig. 4*B*). This may be the antisense RNA that is produced when RDR6 reaches the 5′ end of the cleavage fragment after AGO7-RISC leaves the cleaved 5′ site in 5P3W.

In contrast to the central mismatches in the 5′ site, the conserved mismatches in the base pairing between the 3′ end of miR390 and the 3′ miR390-binding site was critical for both antisense strand synthesis and tasiRNA biogenesis (5W3P; Fig. 4*C*). Given that the 3′ site of 5W3P was efficiently cleaved by the miR390-AGO7-RISC just like wild-type TAS3 RNA (5W3W) (Fig. 4*C*), we speculate that the additional base pairings compromise a downstream step(s). To test if the RDR6 recruitment is impaired by this mutation, we performed coimmunoprecipitation with AGO7 as a bait. This experiment showed that RDR6 can associate with 5W3P in the presence of miR390-AGO7 RISC (Fig. 4*D*), suggesting that the extensive base pairing at the 3′ miR390-binding site compromises the dsRNA conversion step (rather than recruitment of RDR6). Interestingly, SGS3 was more efficiently pulled down in the presence of 5W3P than 5W3W (Fig. 4*D*). This suggests that SGS3 is recruited not only to the 5′ miR390 binding site but also to the 3′ miR390 binding site in 5W3P. Indeed, our recent study showed that the extensive base pairing between the 3′ end region of miR390 and the 5′ binding site promotes stable binding of SGS3 to the target site (28). Thus, we hypothesized that the SGS3-miR390-AGO7 complex binds to the 3′ end of the 5′ cleavage fragment of 5W3P, thereby blocking the initiation of dsRNA synthesis by RDR6. To test this idea, we sought to observe the interaction between the SGS3-miR390-AGO7 complex and the 3′ miR390-binding sites of 5W3P by RNA immunoprecipitation analysis (Fig. 5*A*). As the 5′ miR390 binding site of TAS3 by itself can bind to SGS3 and AGO7-RISC, we introduced mutations in the seed region of the 5′ site of 5W3P (5m3P; Fig. 5*A*). After AGO7-RISC assembly in BY-2 lysate, cap-labeled TAS3 mutants (5m3W, 5m3m, or 5m3P) were incubated in the reaction. Then, SGS3 and FLAG-tagged AGO7 were pulled down with anti-NtSGS3 and anti-FLAG antibodies, respectively, and the coimmunoprecipitated cap-labeled TAS3 fragments were detected (Fig. 5*B*). As expected, only a negligible amount of 5m3m was pulled down after immunoprecipitation (Fig. 5*C*). Importantly, the 5′ cleaved fragment of 5m3P was more efficiently coimmunoprecipitated than that of 5m3W by both anti-NtSGS3 and anti-FLAG antibodies (Fig. 5*C*). Thus, the additional 4-nucleotide base pairings promote the association between the 3′ miR390 cleavage site and the SGS3-miR390-AGO7 complex. Although a previous study showed that SGS3 promotes association of miR173-AGO1-RISC with the cleavage fragments of TAS2 RNA (29), it is unclear if the same is true for the binding between miR390-AGO7-RISC and the cleavage fragments of 5m3P. When we predicted the free energies of the heterodimers between the 3′ half of miRNAs and the 5′ half of the binding sites ($\Delta G_{binding}$), we found that the base pairing between miR390 and the 3′ end of the cleavage fragment of 5m3P is more stable ($\Delta G_{binding}$ = −24.19 kcal/mol; Fig. 5*A*) than the corresponding base pairings between miR173 and TAS1/2 ($\Delta G_{binding}$ = −16.1 kcal/mol; *SI Appendix*, Fig. S5) or between miR390 and the wild-type 3′ binding site ($\Delta G_{binding}$ = −12.77 kcal/mol; Fig. 5*A*). Thus, it is possible that the guanine-cytosine (GC)-rich base pairing in the 3′ binding site in 5m3P is sufficient for the stable binding of AGO7-RISC to the end of the cleavage fragment without the help of SGS3 protein. To investigate whether SGS3 recruitment enhances AGO7-RISC binding to the 3′ miR390 cleavage site of 5m3P, we performed coimmunoprecipitation experiments using the NtSGS3-depleted lysate with supplementation of different concentrations of the recombinant AtSGS3 proteins. The binding between AGO7-RISC and 5m3P was not promoted by the addition of AtSGS3 protein (Fig. 5*D*). Thus, the GC-rich base pairing can retain AGO7-RISC at the 3′ end of the cleavage fragment for extended periods of time even without SGS3. Taken all together, the evolutionarily conserved mismatches in the 3′ miR390 binding site are essential to initiate dsRNA synthesis by promoting destabilization and rapid release of AGO7-RISC from the cleavage site.

Discussion

Here, we developed an in vitro system that successfully recapitulates the widely conserved plant endogenous secondary siRNA biogenesis pathway and allows its mechanistic dissection. Using this system, we demonstrated that a dsRNA-binding protein, SGS3, and a putative homolog of a human mRNA export factor, SDE5, facilitate recruitment of RDR6 to the primary miRNA bound precursor RNA. Furthermore, we found that removal of the poly(A)-tail enhances initiation of RDR6-mediated dsRNA synthesis but not the recruitment of RDR6. Moreover, we revealed that the evolutionarily conserved mismatches between the 3′ end of miR390 and the 3′ miR390-binding site are essential to initiate dsRNA synthesis by promoting rapid release of AGO7-RISC from the cleavage site.

Our reconstituted tasiRNA biogenesis system uses the 17,000 × *g* supernatant of tobacco cell extract (Fig. 1), in which most of the membrane fraction has been removed. This suggests that strict subcellular localization of tasiRNA factors is not absolutely required for small RNA amplification and that this reaction cascade, including targeting by AGO7/1-RISC, dsRNA conversion by RDR6, and dicing by DCLs, can occur in soluble fractions. However, it is still possible that some microsomes remain in the 17,000 × *g* supernatant and act as scaffolds for the formation of the siRNA body-like structures in vitro. Future studies are warranted to examine the interplay between membranes, siRNA body formation, and tasiRNA production in our in vitro system.

Prior work shows that SGS3 plays a role in stabilizing the 5′ and 3′ TAS1/2 fragments generated by miR173-directed cleavage (29). Additionally, by binding to either the miR390-AGO7 or miR173-AGO1 complexes, SGS3 stalls ribosomes on TAS3 or TAS1/2, promoting tasiRNA production (28). In this study, we identified a critical role for SGS3 as essential for RDR6 recruitment to TAS precursors (Figs. 2*G* and 5). Together, the multifunctional roles of SGS3 maximize secondary siRNA production from TAS precursors. In addition to SGS3, we also revealed a role for SDE5 in recruitment of RDR6 (Figs. 2*G* and 5). Coimmunoprecipitation assays suggested that SDE5 transiently interacts with AGO7, SGS3, and RDR6 (*SI Appendix*, Fig. S3*C*) and acts as a connector between these factors. Previous reports demonstrated that SGS3, RDR6, and AGO7 are colocalized in siRNA bodies (26, 27). In addition, a recent study showed that SGS3 forms droplets with liquid-like properties (52). Based on these results, we propose a model for RDR6 recruitment to the precursor RNAs of phasi/tasiRNAs. First, the precursor RNA bound to the initiator RISC—22-nt small RNA-loaded AGO1 or miR390-AGO7—interacts with SGS3s, which form liquid droplets. Second, SDE5 pulls RDR6 into the droplets by transiently interacting with AGO1/7, SGS3, and RDR6. Third, the locally concentrated RDR6s recognize

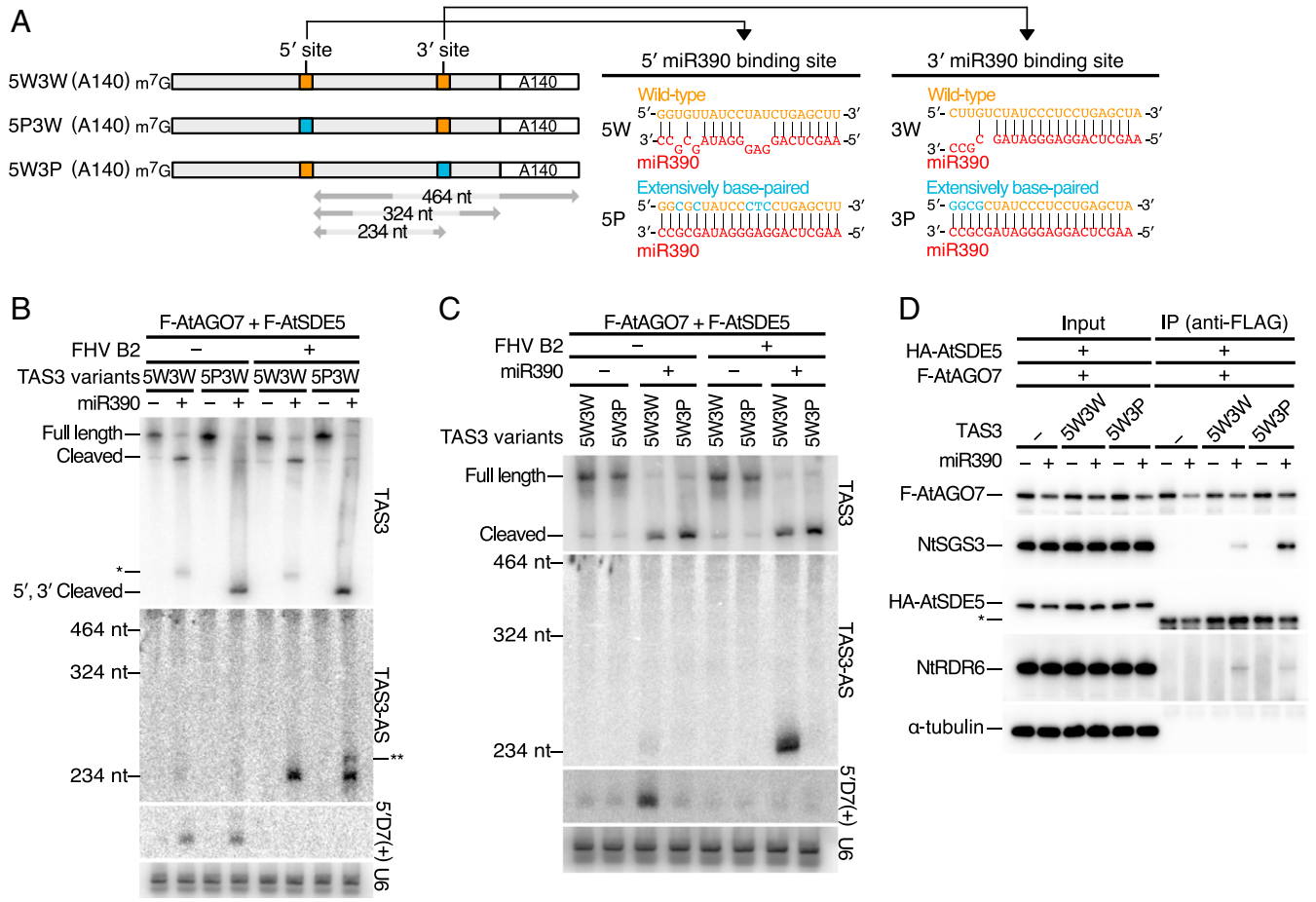

Fig. 4. The mismatches in the 3′ miR390 binding site are essential for dsRNA synthesis. (*A*, *Left*) A schematic illustrating wild-type TAS3 and the TAS3 variants with compensatory mutations in the 5′ or 3′ binding site (5P3W and 5W3P). The base-pairing configurations between miR390 (red) and the wild-type miR390 binding sites (orange) or the binding sites with compensatory mutations (blue). (*B*) In vitro tasiRNA biogenesis with wild-type TAS3 (5W3W) or 5P3W in the presence or absence of FHV B2. The compensatory mutations in the 5′ miR390 binding site did not affect tasiRNA production. The single asterisk indicates a degradation intermediate of wild-type TAS3 only detected in the presence of AGO7-RISC. The double asterisk indicates the longer antisense TAS3 RNA specifically detected when the 5′ miR390 binding was cleaved by AGO7-RISC. TAS3 sense RNA, TAS3 antisense RNA, and 5′D7 (+) tasiRNA were detected by northern blotting with specific probes. U6 spliceosomal RNA was used as a loading control. (*C*) In vitro tasiRNA biogenesis with wild-type TAS3 (5W3W) or 5W3P in the presence or absence of FHV B2. While both 5W3W and 5W3P were efficiently cleaved by the miR390-AGO7-RISC, neither the complementary strand nor 5′D7 (+) tasiRNA were produced from TAS3 5W3P target RNA. TAS3 sense RNA, TAS3 antisense RNA, and 5′D7 (+) tasiRNA were detected by northern blotting with specific probes. U6 spliceosomal RNA was used as a loading control. (*D*) Coimmunoprecipitation experiments with F-AtAGO7 in the presence of wild-type TAS3 (5W3W) or its variant with compensatory mutations in the 3′ miR390 binding site (5W3P) shown in *A*. F-AtAGO7 was immunoprecipitated (IP) using anti-FLAG antibody, and blotted with anti-FLAG, anti-SGS3, anti-HA, anti-NtRDR6, or anti-tubulin antibodies. NtRDR6 and abundant NtSGS3 were coimmunoprecipitated with F-AtAGO7 in the presence of 5W3P in a manner dependent on the miR390 duplex. The asterisk indicates nonspecific bands. α-tubulin was used as a loading control as well as a negative control for coimmunoprecipitation experiments.

the 3′ end of the precursor RNAs (Fig. 6). The siRNA bodies formed by SGS3, special RISC, and SDE5 might also activate RDR6 and/or protect the synthesized dsRNAs from unwanted nucleases. Future studies combining our in vitro system and imaging approaches will test this model.

It is known that TAS3 tasiRNAs have specific "hotspots" of increased accumulation between the two miR390 binding sites in *Arabidopsis* (Fig. 1*E*) (33). Our in vitro system mimics this pattern of tasiRNA biogenesis (Fig. 1*E* and *SI Appendix*, Fig. S1*E*). Interestingly, the most prominent hotspot overlaps with 5′D7(+)—the most physiologically important TAS3 tasiRNA—both in vivo and in vitro (Fig. 1*E*). This suggests that the biologically important small RNAs produced from this region are selectively stabilized by an unknown mechanism. The most plausible explanation for this is that endogenous AGO proteins specifically load a subset of siRNAs, protecting them from degradation by nucleases. The hotspot contains four consecutive U nucleotides, whereas 18 to 21 nt downstream are four consecutive Cs. These features are ideal for AGO1-RISC assembly; plant AGO1 has a binding preference for 5′ U small RNAs (53, 54). In addition, AGO proteins generally preferentially select the small RNA strand with lower thermodynamic stability at the 5′ end (low-GC content) (55). Thus, the unique sequence surrounding the hotspot may enhance selective loading and stabilization by AGO1.

Our in vitro tasiRNA production system demonstrates that a nonpolyadenylated 3′ end is preferred as an initiation site for dsRNA conversion rather than a polyadenylated one (Fig. 3 and *SI Appendix*, Fig. S2). This can be explained by the intrinsic properties of RDR6; recombinant RDR6 selects poly(A)-less mRNAs over polyadenylated mRNAs as templates at the initiation step of complementary strand RNA synthesis (17). We envision that the 3′ site cleavage (which effectively removes the poly(A) tail) in the TAS3 pathway creates a non-poly(A) 3′ end, thus enhancing tasiRNA production (Fig. 5). A previous study has suggested that the 3′ miR390 site is essential

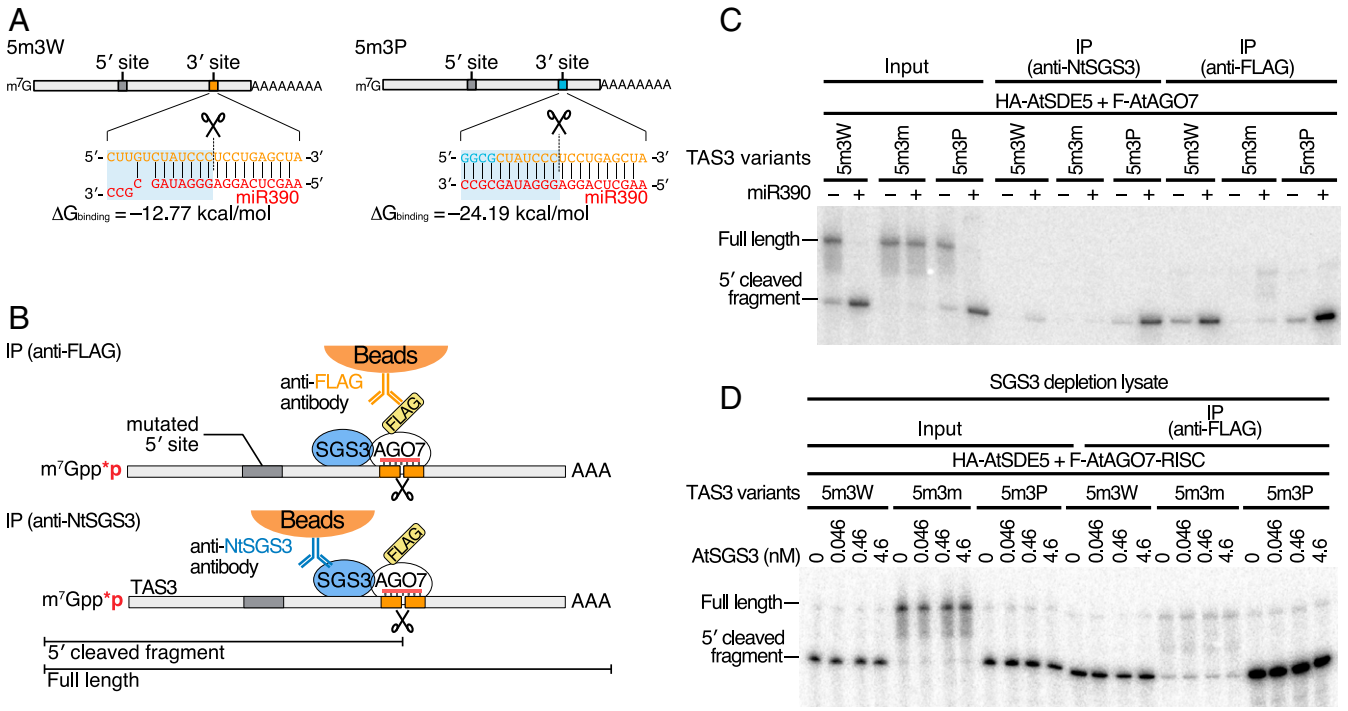

Fig. 5. The evolutionarily conserved mismatches in the 3′ miR390 binding site promotes rapid release of AGO7-RISC from the cleavage site. (*A*) A schematic illustrating TAS3 variants with the seed-mutated 5′ binding site and the wild-type 3′ binding site (5m3W) or that with the seed-mutated 5′ binding site and compensatory mutations in the 3′ miR390 binding site (5m3P). The base-pairing configurations between miR390 (red) and wild-type miR390 binding sites (orange) or binding sites with compensatory mutations (blue). The light blue shaded boxes indicate heterodimers of the 3′ half of miR390 and the 5′ half of the binding sites. Scissors indicate cleavage sites. $\Delta G_{binding}$ indicates the free energies of the heterodimers of the 3′ half of miRNAs and the 5′ half of the binding sites. (*B*) Schematic illustrating RNA coimmunoprecipitation assay using the anti-FLAG antibody (*Upper*) and anti-SGS3 antibody (*Lower*). (*C*) RNA coimmunoprecipitation experiments with 3×FLAG-AtAGO7 (F-AtAGO7) and NtSGS3. Cap-labeled TAS3 RNAs (5m3W, 5m3m, and 5m3P) were detected. The 5′ fragment of 5m3P was more efficiently coimmunoprecipitated by anti-FLAG antibody and anti-NtSGS3 antibody than that of 5m3W, suggesting that SGS3-miR390-AGO7-RISC remains at the 3′ binding site after target cleavage. (*D*) RNA coimmunoprecipitation experiments with F-AtAGO7 in the NtSGS3-depleted lysate. The supplementation of AtSGS3 protein did not promote the interaction between AGO7-RISC and the 5′ cleavage fragment of 5m3P.

for setting the proper phasing register (34). Thus, the cleavable 3′ miR390 site has a dual role in determination of the initiation site for phase of tasiRNAs and promotion of dsRNA synthesis, both of which maximize the production of functional tasiRNAs. Although poly(A) removal also enhances dsRNA synthesis in the one-hit TAS1 pathway (*SI Appendix*, Fig. S2), detectable levels of dsRNAs and tasiRNAs were produced when polyadenylated TAS1 was added into the cell-free system (*SI Appendix*, Fig. S2). This suggests a two-step production mechanism of tasiRNAs from TAS1; low levels of tasiRNAs are first produced from polyadenylated TAS1 RNA, then the 21-nt tasiRNAs cleave TAS1 in cis to generate non-poly(A) template that efficiently produce tasiRNAs (Fig. 5). Indeed, it is known that some tasiRNAs, including 3′D6 (−) and 3′D10 (−) from TAS1c, direct secondary target cleavage of TAS1/2 RNAs at the 3′ side of the miR173 binding site, thereby creating a non-poly(A) 3′ end (*SI Appendix*, Fig. S5) (39).

In this study, we shed light on the "dark side" of the two-hit pathway: if base pairing between the 3′ targeting site and the primary miRNA is too strong, RISC remains at the 3′ miRNA binding site even after the target cleavage, which completely blocks both dsRNA synthesis and tasiRNA production. This finding in turn suggests that TAS3 mRNA cleverly evades the negative effect of the 3′ miR390 binding site by appropriately harboring 4-nt mismatches there. Interestingly, the base pairs between the 3′D6 (−)/3′D10 (−) TAS1c tasiRNAs and the 3′ end of the fragments cleaved at the secondary cleavage sites of TAS1/2 RNAs are as weak as that between miR390 and the 3′ end of the cleavage fragment of wild-type TAS3 RNA (Fig. 5*A* and *SI Appendix*, Fig. S5). This suggests that the AU-rich sequences or the mismatches in GC-rich sequences are required for the secondary cleavage site to trigger tasi/phasiRNA biogenesis; otherwise, the strong base pairing between small RNAs and the end of the cleavage fragment retains RISCs at the 3′ end for extended periods of time, resulting in inhibition of dsRNA synthesis by RDR6.

Taken together, we have revealed key mechanisms underlying phasi/tasiRNA biogenesis. Our in vitro system will pave the way for understanding the molecular bases of RNA silencing amplification, including not only phasi/tasiRNA biogenesis but also transgene-triggered and virus-triggered gene silencing in plants.

Materials and Methods

General Methods. Preparation of lysate from tobacco BY-2 cells, substrate mixture (containing adenosine triphosphate [ATP], ATP-regeneration system, amino acid mixture), 1× lysis buffer (30 mM 2-(4-(2-hydroxyethyl)piperazin-1-yl)ethanesulfonic acid [Hepes] at pH 7.4, 100 mM potassium acetate, 2 mM magnesium acetate), and small RNA duplexes have been previously described in detail (43). Anti-NtRDR6 was raised in rabbits using synthetic peptides (NH_2-CLGPENPYRLNQRRRTTM-COOH) as antigens (Medical and Biological Laboratories).

In Vitro tasiRNA Biogenesis Assay. Basically, 10 μL of BY-2 lysate, 5 μL of substrate mixture, and 0.5 μL each of 1 μM F-AtAGO7 mRNA and 1 μM F-AtSDE5 mRNA were mixed and incubated at 25 °C. After 30 min, 1 μL of 1 μM miR390/miR390* duplex was added and further incubated at 25 °C for 1.5 h. The reaction was mixed and incubated at 25 °C for 10 min with or without 1 μL of 1 μM viral silencing suppressor FHV-B2 recombinant protein, purified as previously described (56). Next, 1 μL of 40 nM TAS3 RNAs was added to the reaction mixture and incubated at 25 °C for 30 min. Aliquots of the reaction mixtures were used for Western blotting by adding sodium dodecyl sulfate (SDS) protein sample buffer (40% glycerol, 240 mM Tris·HCl pH 6.8, 8% SDS, 0.04% bromophenol blue, and dithiothreitol), and for northern blotting

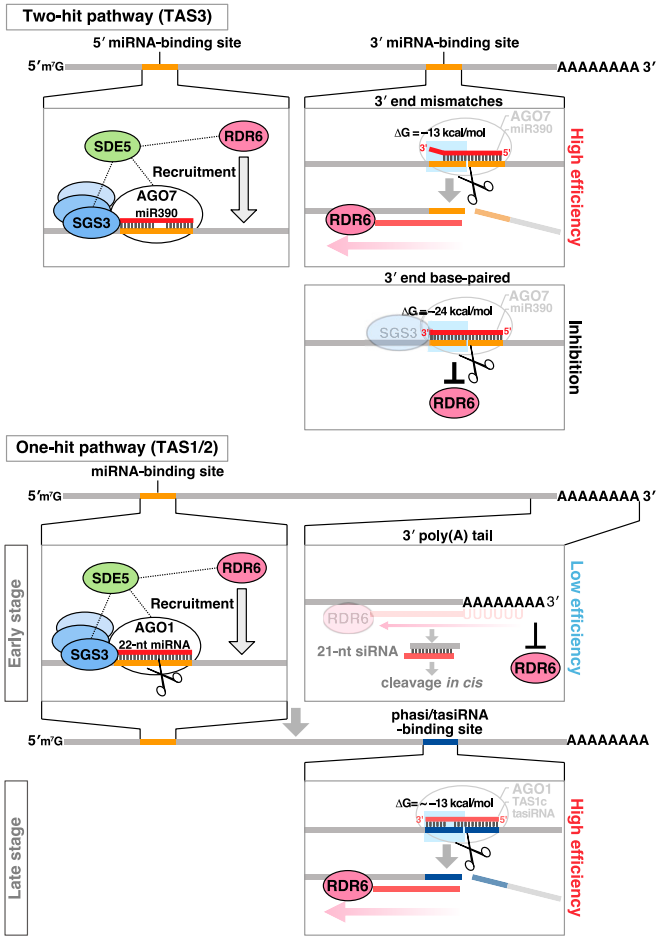

Fig. 6. A model for the initiation of tasiRNA biogenesis. The precursor RNA bound to the initiator RISC—22-nt small RNA-loaded AGO1 or miR390-AGO7—interacts with SGS3s, which form liquid droplets. Then, SDE5 pulls RDR6 into the droplets by transiently interacting with AGO1/7, SGS3, and RDR6. In the two-hit pathway, removal of poly(A) tail by the cleavage of the 3′ target site promotes dsRNA synthesis. In this process, the 4-nucleotide mismatches between miR390 and the 3′ site are critical for the rapid release of the SGS3-miR390-AGO7 complex from the cleavage site. If the complementarity is too strong, the complex remaining at the 3′ cleavage site completely inhibits both dsRNA synthesis and tasiRNA production. In the one-hit pathway, although the poly(A) tail represses dsRNA synthesis, a small amount of tasiRNAs are generated. Such a low level of tasiRNAs cleave the target mRNA in cis, creating nonpolyadenylated 3′ ends favored by RDR6. As the heteroduplex of the 3′ half of tasiRNAs and the 5′ half of these binding sites are as weak as that of the 3′ half of miR390 and the 5′ half of the 3′ binding site in wild-type TAS3, tasiRNA-AGO1 complex can rapidly dissociate from the cleavage site.

after deproteinization with proteinase K (Nacalai Tesque, Inc.) and ethanol precipitation followed by dissolving the pellet in formamide dye (49% formamide, 5 mM ethylenediamine tetraacetic acid [EDTA], 0.01% xylene cyanol, and 0.01% bromophenol blue). For Fig. 1 *C* and *D* and *SI Appendix*, Fig. S1*B*, 12 μL of BY-2 lysate, 6 μL of substrate mixture, 0.6 μL of 1 μM F-AtAGO7 mRNA, 0.6 μL of 1 μM F-AtSDE5 mRNA, 0.5 μL of 0.25 μM F-AtSGS3 mRNA, and 1 μL of 0.5 μM F-AtRDR6 mRNA were used.

Coimmunoprecipitation Assay. The anti-FLAG antibody (Sigma) was immobilized using Dynabeads protein G (Invitrogen) in 1× lysis buffer and rotated at 4 °C for 1 h. After immobilization, the beads were washed 3 times with lysis wash buffer containing 200 mM NaCl and 1% Triton X-100 [polyoxyethylene (10) octylphenyl ether, Wako]. Afterward, the tasiRNA biogenesis assay reaction mixture was added to the beads and rotated at 4 °C for 1 h. The beads were washed with lysis wash buffer three times, and finally, proteins were resuspended in SDS protein sample buffer. For SGS3 immunoprecipitation (Fig. 2*F*), the anti-NtSGS3 antibody (29) was added directly to the tasiRNA biogenesis reaction mixture and incubated for 30 min on ice. After incubation, Dynabeads protein G (Invitrogen), washed with lysis wash buffer, was added to the reaction mixture and rotated at 4 °C for 30 min. The wash step was performed as outlined. For RNA immunoprecipitation, cap-labeled TAS3 target RNAs were used (Fig. 4*D*). After wash step, the beads were incubated with 1× lysis buffer containing proteinase K (200 ng/uL) at 55 °C for 10 min. Finally, the samples were resuspended in the same volume of formamide dye (10 mM EDTA pH 8.0, 98% [wt/vol] deionized formamide, 0.025% [wt/vol] xylene cyanol, and 0.025% bromophenol blue). After incubation at 95 °C for 2 min, the coimmunoprecipitated RNAs were separated on an 5% polyacrylamide denaturing gel.

Immunodepletion of Endogenous SGS3. Immunodepletion of NtSGS3 from BY-2 lysate was performed as previously described (28).

Western Blot Assay. The reactions, which were resuspended in 1× SDS protein sample buffer, were heated at 95 °C for 5 min. After electrophoresis, the proteins were transferred onto polyvinylidene difluoride membrane (Merck) via a semidry transfer method. The membrane was incubated with blocking buffer (1% skim milk and 1× Tris buffered saline with Tween 20 [TBS-T]) at room temperature for 1 h and supplemented with anti-FLAG antibodies (Sigma, #F1804; 1:10,000 dilution) or anti-HA antibodies (abcam, #ab130275; 1:10,000 dilution), anti-tubulin antibodies (Sigma, #T6074; 1:10,000 dilution), anti-NtSGS3 antibodies (29) (1:10,000 dilution), and anti-NtRDR6 antibodies (1:5,000 dilution) at 4 °C overnight. The membrane was washed with 1× TBS-T and then incubated with blocking buffer (1% skim milk and 1× TBS-T) with anti-mouse immunoglobulin G (IgG)–horseradish peroxidase (HRP) antibodies (MBL, #330; 1:25,000 dilution) or anti-rabbit IgG-HRP antibodies (Jackson, #111-035-003; 1:20,000 dilution) at room temperature for 1 h. After washing with 1× TBS-T, the membrane was treated with Immobilon Western Chemiluminescent HRP Substrate (Millipore). Images were acquired using the Imager 600 (Amersham) or FUSION FX (VILBER).

Preparation of Probes for Northern Blot Assay. DNA oligo probes (*SI Appendix*, Table S4) were phosphorylated using T4 polynucleotide kinase (TaKaRa) with [γ-^{32}P]-ATP. Multiple DNA oligos (*SI Appendix*, Table S4) were mixed and radiolabeled as described for the detection of sense, antisense TAS3a, and antisense TAS1a.

Northern Blot Assay. To detect U6 spliceosomal RNA and tasiRNAs, RNAs were separated on an 18% polyacrylamide denaturing gel and transferred onto a Hybond-N membrane (GE Healthcare) using semidry transfer. The 1-ethyl-3-(3-dimethylaminopropyl)carbodiimide (EDC) cross-linking was used to fix RNA to the Hybond-N membrane, as described previously (57). Hybond-N membrane was placed onto filter paper soaked in EDC solution and incubated at 60 °C for 1 h. To detect TAS3 mRNA, antisense TAS3 mRNA, TAS1 mRNA, and antisense TAS1 mRNA, a 5% polyacrylamide denaturing gel and a Hybond-N+ membrane (GE Healthcare) were used. RNAs were fixed to the Hybond-N+ membrane by ultraviolet cross-linking. Membranes were placed in a hybridization bottle with 10 mL of PerfectHyb Plus Hybridization buffer (Sigma). The bottle was then preincubated at 42 °C for more than 5 min in the hybridization oven. After preincubation, a radiolabeled probe was hybridized with membranes overnight. The membrane was washed with low stringency buffer (2× saline-sodium citrate [SSC] and 0.1% SDS) at room temperature for more than 5 min and then washed with high stringency buffer (0.1× SSC and 0.1% SDS) at the hybridization temperature for 20 min. Images were acquired using the Typhoon FLA 7000 IP (GE Healthcare). The markers for northern blotting used in this study are listed in *SI Appendix*, Table S5.

Small RNA-seq. Total RNA was extracted from 3-d-old Col-0 and *sgs3-11* (21) *Arabidopsis* seedlings and BY-2 lysate with TRIzol reagent. Followed by gel purification, 19 to 28 nt length small RNAs were gel extracted from total RNAs. Small RNA libraries were prepared by using NEBNext Multiplex Small RNA Library Prep Set for Illumina (NEB) and analyzed by Illumina HiSEq 4000.

Sequence Analysis of tasiRNAs. After removal of adaptor sequences by cutadapt (58), small RNA sequence reads of 20 to 29 nt length were mapped to the TAS3a sequence used in the tasiRNA biogenesis assay using the FASTX-Toolkit (http://hannonlab.cshl.edu/fastx_toolkit/) and Bowtie (59) allowing for up to one mismatch. Sequence Alignment Map (SAM) files were converted to BAM files using SAMtools (60) and then to BED files with BEDTools (61). Processed data were transferred to R, and length distribution and the 5′-end position for each siRNA were mapped onto the TAS3 mRNA using the ggplot2 package.

Prediction of the Free Energies of Heterodimers. The free energies of heterodimers of the 3′ half of small RNAs and the 5′ half of binding sites were predicted at 25 °C via the Vienna RNA Websuite (62).

Data Availability. The sequencing data reported in this paper are publicly available in DNA Data Bank of Japan (DDBJ; http://www.ddbj.nig.ac.jp/) under the accession numbers DRA009601 for in vitro data and DRA009602 for in vivo data.

ACKNOWLEDGMENTS. We thank Manabu Yoshikawa for sharing unpublished data and providing anti-NtSGS3 and anti-NtRDR6, Mariko Watanabe for production of FHV B2 protein, Kaori Kiyokawa for experimental assistance, and Life Science Editors for editorial assistance. We also thank all the members of the Y.T. laboratory for discussion and critical comments on the manuscript. This work was supported in part by JST, PRESTO (Grant JPMJPR18K2 to H.-o.I.), Grant-in-Aid for Young Scientists (A) (Grant 16H06159 to H.-o.I.), Grant-in-Aid for Scientific Research on Innovative Areas ("Nascent-chain Biology") (Grant 26116003 to H.-o.I.), Grant-in-Aid for Challenging Exploratory Research (Grant 15K14444 to H.-o.I.), Grant-in-Aid for Japan Society for the Promotion of Science (JSPS) Fellows 16J07290 (to K.B.), and Grant-in-Aid for JSPS Fellows 20J11529 (to Y.S.). DNA libraries were sequenced by the Vincent J. Coates Genomics Sequencing Laboratory at University of California, Berkeley, supported by an NIH S10 OD018174 Instrumentation Grant.

1. M. Ghildiyal, P. D. Zamore, Small silencing RNAs: An expanding universe. *Nat. Rev. Genet.* **10**, 94–108 (2009).
2. N. G. Bologna, O. Voinnet, The diversity, biogenesis, and activities of endogenous silencing small RNAs in *Arabidopsis*. *Annu. Rev. Plant Biol.* **65**, 473–503 (2014).
3. H. Kobayashi, Y. Tomari, RISC assembly: Coordination between small RNAs and Argonaute proteins. *Biochim. Biophys. Acta* **1859**, 71–81 (2016).
4. S. L. Ameres, P. D. Zamore, Diversifying microRNA sequence and function. *Nat. Rev. Mol. Cell Biol.* **14**, 475–488 (2013).
5. D. P. Bartel, MicroRNAs: Target recognition and regulatory functions. *Cell* **136**, 215–233 (2009).
6. H. O. Iwakawa, Y. Tomari, The functions of MicroRNAs: mRNA decay and translational repression. *Trends Cell Biol.* **25**, 651–665 (2015).
7. D. C. Baulcombe, Molecular biology. Amplified silencing. *Science* **315**, 199–200 (2007).
8. T. Dalmay, A. Hamilton, S. Rudd, S. Angell, D. C. Baulcombe, An RNA-dependent RNA polymerase gene in *Arabidopsis* is required for posttranscriptional gene silencing mediated by a transgene but not by a virus. *Cell* **101**, 543–553 (2000).
9. Y. Dang, Q. Yang, Z. Xue, Y. Liu, RNA interference in fungi: Pathways, functions, and applications. *Eukaryot. Cell* **10**, 1148–1155 (2011).
10. H. Nakayashiki, N. Kadotani, S. Mayama, Evolution and diversification of RNA silencing proteins in fungi. *J. Mol. Evol.* **63**, 127–135 (2006).
11. T. Sijen *et al*., On the role of RNA amplification in dsRNA-triggered gene silencing. *Cell* **107**, 465–476 (2001).
12. S. E. Castel, R. A. Martienssen, RNA interference in the nucleus: Roles for small RNAs in transcription, epigenetics and beyond. *Nat. Rev. Genet.* **14**, 100–112 (2013).
13. J. T. Cuperus *et al*., Unique functionality of 22-nt miRNAs in triggering RDR6-dependent siRNA biogenesis from target transcripts in *Arabidopsis*. *Nat. Struct. Mol. Biol.* **17**, 997–1003 (2010).
14. H. M. Chen *et al*., 22-Nucleotide RNAs trigger secondary siRNA biogenesis in plants. *Proc. Natl. Acad. Sci. U.S.A.* **107**, 15269–15274 (2010).
15. Y. Liu, C. Teng, R. Xia, B. C. Meyers, PhasiRNAs in plants: Their biogenesis, genic sources, and roles in stress responses, development, and reproduction. *Plant Cell* **32**, 3059–3080 (2020).
16. J. Curaba, X. Chen, Biochemical activities of *Arabidopsis* RNA-dependent RNA polymerase 6. *J. Biol. Chem.* **283**, 3059–3066 (2008).
17. K. Baeg, H. O. Iwakawa, Y. Tomari, The poly(A) tail blocks RDR6 from converting self mRNAs into substrates for gene silencing. *Nat. Plants* **3**, 17036 (2017).
18. M. Yoshikawa, A. Peragine, M. Y. Park, R. S. Poethig, A pathway for the biogenesis of trans-acting siRNAs in *Arabidopsis*. *Genes Dev.* **19**, 2164–2175 (2005).
19. Z. Xie, E. Allen, A. Wilken, J. C. Carrington, DICER-LIKE 4 functions in trans-acting small interfering RNA biogenesis and vegetative phase change in *Arabidopsis* thaliana. *Proc. Natl. Acad. Sci. U.S.A.* **102**, 12984–12989 (2005).
20. I. Hernandez-Pinzon *et al*., SDE5, the putative homologue of a human mRNA export factor, is required for transgene silencing and accumulation of trans-acting endogenous siRNA. *Plant J.* **50**, 140–148 (2007).
21. A. Peragine, M. Yoshikawa, G. Wu, H. L. Albrecht, R. S. Poethig, SGS3 and SGS2/SDE1/RDR6 are required for juvenile development and the production of trans-acting siRNAs in *Arabidopsis*. *Genes Dev.* **18**, 2368–2379 (2004).
22. F. Vazquez *et al*., Endogenous trans-acting siRNAs regulate the accumulation of *Arabidopsis* mRNAs. *Mol. Cell* **16**, 69–79 (2004).
23. V. Gasciolli, A. C. Mallory, D. P. Bartel, H. Vaucheret, Partially redundant functions of *Arabidopsis* DICER-like enzymes and a role for DCL4 in producing trans-acting siRNAs. *Curr. Biol.* **15**, 1494–1500 (2005).
24. T. Elmayan *et al*., A neomorphic sgs3 allele stabilizing miRNA cleavage products reveals that SGS3 acts as a homodimer. *FEBS J.* **276**, 835–844 (2009).
25. E. Glick *et al*., Interaction with host SGS3 is required for suppression of RNA silencing by tomato yellow leaf curl virus V2 protein. *Proc. Natl. Acad. Sci. U.S.A.* **105**, 157–161 (2008).
26. N. Kumakura *et al*., SGS3 and RDR6 interact and colocalize in cytoplasmic SGS3/RDR6-bodies. *FEBS Lett.* **583**, 1261–1266 (2009).
27. V. Jouannet *et al*., Cytoplasmic *Arabidopsis* AGO7 accumulates in membrane-associated siRNA bodies and is required for ta-siRNA biogenesis. *EMBO J.* **31**, 1704–1713 (2012).
28. H. O. Iwakawa *et al*., Ribosome stalling caused by the Argonaute-microRNA-SGS3 complex regulates the production of secondary siRNAs in plants. *Cell Rep.* **35**, 109300 (2021).
29. M. Yoshikawa *et al*., 3′ fragment of miR173-programmed RISC-cleaved RNA is protected from degradation in a complex with RISC and SGS3. *Proc. Natl. Acad. Sci. U.S.A.* **110**, 4117–4122 (2013).
30. M. Yoshikawa *et al*., A short open reading frame encompassing the microRNA173 target site plays a role in trans-acting small interfering RNA biogenesis. *Plant Physiol.* **171**, 359–368 (2016).
31. R. Xia, J. Xu, B. C. Meyers, The emergence, evolution, and diversification of the miR390-*TAS3-ARF* pathway in land plants. *Plant Cell* **29**, 1232–1247 (2017).
32. M. D. Howell *et al*., Genome-wide analysis of the RNA-DEPENDENT RNA POLYMERASE6/DICER-LIKE4 pathway in *Arabidopsis* reveals dependency on miRNA- and tasiRNA-directed targeting. *Plant Cell* **19**, 926–942 (2007).
33. M. J. Axtell, C. Jan, R. Rajagopalan, D. P. Bartel, A two-hit trigger for siRNA biogenesis in plants. *Cell* **127**, 565–577 (2006).
34. F. F. de Felippes, A. Marchais, A. Sarazin, S. Oberlin, O. Voinnet, A single miR390 targeting event is sufficient for triggering TAS3-tasiRNA biogenesis in *Arabidopsis*. *Nucleic Acids Res.* **45**, 5539–5554 (2017).
35. E. Allen, Z. Xie, A. M. Gustafson, J. C. Carrington, microRNA-directed phasing during trans-acting siRNA biogenesis in plants. *Cell* **121**, 207–221 (2005).
36. N. Fahlgren *et al*., Regulation of AUXIN RESPONSE FACTOR3 by TAS3 ta-siRNA affects developmental timing and patterning in *Arabidopsis*. *Curr. Biol.* **16**, 939–944 (2006).
37. Z. Luo, Z. Chen, Improperly terminated, unpolyadenylated mRNA of sense transgenes is targeted by RDR6-mediated RNA silencing in *Arabidopsis*. *Plant Cell* **19**, 943–958 (2007).
38. F. F. de Felippes *et al*., The key role of terminators on the expression and post-transcriptional gene silencing of transgenes. *Plant J.* **104**, 96–112 (2020).
39. R. Rajeswaran *et al*., Sequencing of RDR6-dependent double-stranded RNAs reveals novel features of plant siRNA biogenesis. *Nucleic Acids Res.* **40**, 6241–6254 (2012).
40. E. Marin *et al*., miR390, *Arabidopsis* TAS3 tasiRNAs, and their AUXIN RESPONSE FACTOR targets define an autoregulatory network quantitatively regulating lateral root growth. *Plant Cell* **22**, 1104–1117 (2010).
41. Y. Endo, H. O. Iwakawa, Y. Tomari, *Arabidopsis* ARGONAUTE7 selects miR390 through multiple checkpoints during RISC assembly. *EMBO Rep.* **14**, 652–658 (2013).
42. H. O. Iwakawa, Y. Tomari, Molecular insights into microRNA-mediated translational repression in plants. *Mol. Cell* **52**, 591–601 (2013).
43. Y. Tomari, H. O. Iwakawa, In vitro analysis of ARGONAUTE-mediated target cleavage and translational repression in plants. *Methods Mol. Biol.* **1640**, 55–71 (2017).
44. T. Iki *et al*., In vitro assembly of plant RNA-induced silencing complexes facilitated by molecular chaperone HSP90. *Mol. Cell* **39**, 282–291 (2010).
45. K. Komoda, S. Naito, M. Ishikawa, Replication of plant RNA virus genomes in a cell-free extract of evacuolated plant protoplasts. *Proc. Natl. Acad. Sci. U.S.A.* **101**, 1863–1867 (2004).
46. T. Iki, M. A. Tschopp, O. Voinnet, Biochemical and genetic functional dissection of the P38 viral suppressor of RNA silencing. *RNA* **23**, 639–654 (2017).
47. J. Schuck, T. Gursinsky, V. Pantaleo, J. Burgyán, S. E. Behrens, AGO/RISC-mediated antiviral RNA silencing in a plant in vitro system. *Nucleic Acids Res.* **41**, 5090–5103 (2013).
48. J. A. Chao *et al*., Dual modes of RNA-silencing suppression by Flock House virus protein B2. *Nat. Struct. Mol. Biol.* **12**, 952–957 (2005).
49. J. K. Seo, S. J. Kwon, A. L. Rao, Molecular dissection of Flock house virus protein B2 reveals that electrostatic interactions between N-terminal domains of B2 monomers are critical for dimerization. *Virology* **432**, 296–305 (2012).
50. G. Singh *et al*., Suppression of RNA silencing by Flock house virus B2 protein is mediated through its interaction with the PAZ domain of Dicer. *FASEB J.* **23**, 1845–1857 (2009).
51. R. Rajeswaran, M. M. Pooggin, RDR6-mediated synthesis of complementary RNA is terminated by miRNA stably bound to template RNA. *Nucleic Acids Res.* **40**, 594–599 (2012).
52. E. Y. Kim *et al*., Ribosome stalling and SGS3 phase separation prime the epigenetic silencing of transposons. *Nat. Plants* **7**, 303–309 (2021).
53. S. Mi *et al*., Sorting of small RNAs into *Arabidopsis* argonaute complexes is directed by the 5′ terminal nucleotide. *Cell* **133**, 116–127 (2008).
54. A. Takeda, S. Iwasaki, T. Watanabe, M. Utsumi, Y. Watanabe, The mechanism selecting the guide strand from small RNA duplexes is different among argonaute proteins. *Plant Cell Physiol.* **49**, 493–500 (2008).
55. A. Khvorova, A. Reynolds, S. D. Jayasena, Functional siRNAs and miRNAs exhibit strand bias. *Cell* **115**, 209–216 (2003).
56. M. Watanabe, H. O. Iwakawa, H. Tadakuma, Y. Tomari, Biochemical and single-molecule analyses of the RNA silencing suppressing activity of CrPV-1A. *Nucleic Acids Res.* **45**, 10837–10844 (2017).
57. G. S. Pall, A. J. Hamilton, Improved northern blot method for enhanced detection of small RNA. *Nat. Protoc.* **3**, 1077–1084 (2008).
58. M. Martin, Cutadapt removes adapter sequences from high-throughput sequencing reads. *EMBnet. J.* **17**, 10–12 (2011).
59. B. Langmead, C. Trapnell, M. Pop, S. L. Salzberg, Ultrafast and memory-efficient alignment of short DNA sequences to the human genome. *Genome Biol.* **10**, R25 (2009).
60. H. Li *et al*.; 1000 Genome Project Data Processing Subgroup, The sequence alignment/map format and SAMtools. *Bioinformatics* **25**, 2078–2079 (2009).
61. A. R. Quinlan, I. M. Hall, BEDTools: A flexible suite of utilities for comparing genomic features. *Bioinformatics* **26**, 841–842 (2010).
62. A. R. Gruber, R. Lorenz, S. H. Bernhart, R. Neuböck, I. L. Hofacker, The Vienna RNA websuite. *Nucleic Acids Res.* **36**, W70–W74 (2008).